Preprints of the 19th World Congress
The International Federation of Automatic Control
Cape Town, South Africa. August 24-29, 2014

Improved Counter-Current and Co-Current Guidance of Underactuated Marine Vehicles with Semiglobal Stability Properties

Walter Caharija * **Esten Ingar Grøtli** * **Kristin Y. Pettersen** *

* *Dept. of Engineering Cybernetics, NTNU, NO-7491 Trondheim, Norway. e-mail: {Walter.Caharija, Esten.Grotli, Kristin.Y.Pettersen}@itk.ntnu.no*

Abstract: A control technique for counter-current and co-current guidance of underactuated marine vehicles is revisited and improved. The control system is based on a pure integral guidance law and two feedback controllers, in a cascaded configuration. The sway component of the ocean current in the body frame is viewed as the error signal of the guidance law instead of the absolute sway velocity, as done in the original approach. This makes the vessel search for the two possible yaw angles giving zero current component in sway: the counter-current direction and the co-current direction. The closed loop system has multiple equilibria where the two mentioned directions represent a set of stable equilibrium points and a set of unstable equilibrium points, respectively. Compared to the approach based on the absolute sway velocity, it is possible to achieve stronger stability properties. In particular, while the previous guidance approach considered a simplified model and yielded local exponential stability only, the complete model is analyzed in this paper and uniform semiglobal asymptotic stability as well as uniform local exponential stability are proven. The theoretical results are supported by simulations.

Keywords: underactuated vessel, ocean currents, semiglobal stability, multiple equilibria

1. INTRODUCTION

Remote sensing and automation of operations at sea represent present and future challenges the offshore and maritime industry is facing worldwide. Any improvements in these fields can significantly increase reliability, safety, sustainability and effectiveness of activities such as offshore hydrocarbon production and exploration, fishing, offshore wind power production, shipping and environmental monitoring. In particular, such activities are significantly affected by wind, waves and sea currents, and hence maneuverability of the ships and vehicles involved can be seriously affected. As a result, the field of marine control has delivered valuable solutions and ideas on how to handle and reduce sea loads. In particular, effective disturbance estimation techniques and reliable compensation strategies have been introduced.

Due to their significant effect on marine operations, handling ocean currents has attracted significant attention and many researchers have developed current observers and adaptive techniques to compensate for the disturbances, often embedded into more advanced guidance and control schemes. Such control approaches are introduced for fully actuated as well as underactuated marine vessels and underwater vehicles in Encarnação et al. (2000); Do et al. (2004); Refsnes et al. (2007); Antonelli (2007); Batista et al. (2012); Indiveri et al. (2012) to compensate for the drift in path following and navigation tasks. To render the popular line-of-sight (LOS) guidance law robust with respect to ocean currents, Aguiar and Pascoal (1997) propose a modification based on measurements of the vehicle velocity and integral action is added to the LOS reference generator in Børhaug et al. (2008); Breivik and Fossen (2009); Caharija et al. (2012a,c). Furthermore, the use of predictive ocean models embedded into the mission planning strategy of the vehicle for current compensation/exploitation is discussed in Smith et al. (2011) and Jouffroy et al. (2011).

In this paper the problem of steering a marine vessel against the ocean current or with the ocean current is addressed. This is indeed an interesting problem since an autonomous marine vehicle capable to sense the current and follow the flow could exploit the drift when exact positioning is not as critical as energy efficiency (Smith et al., 2011). In fact, such guidance law makes the vehicle determine the direction that guarantees the minimum energy consumption for a given absolute speed. Moreover, an underwater vehicle that can turn against the flow could, for instance, help locate a hydrothermal vent Yoerger et al. (2007) or detect hydrocarbon leaks from subsea oil and gas installations. Furthermore, a control law for counter-current guidance can be integrated into more complex weather optimal heading/positioning control systems (WOHC-WOPC) since it is meant to steer the vessel against the disturbance. The WOHC and WOPC concepts are thoroughly defined by Fossen and Strand (2001) and enhanced with a geometrically motivated update law in Kjerstad and Breivik (2010) for fully actuated as well as underactuated vessels.

Supported by the Research Council of Norway through the Centers of Excellence funding scheme (project number 223254) and the Strategic University Program (project number 192427).

This paper aims at improving the counter-current/co-current guidance for underactuated autonomous marine vehicles in 3 degrees of freedom (DOF) developed in Caharija et al. (2013). In Caharija et al. (2013) the absolute sway velocity is integrated and represents the actual error signal. This leads to a closed loop pendulum-like system with multiple equilibrium points, where one of the two mentioned directions represent a set of stable equilibrium points and the other a set of unstable equilibrium points. The closed-loop analysis of Caharija et al. (2013), based on Lyapunov perturbation theory, shows only local exponential stability for the stable direction, and neglects the perturbing dynamics of the vessel autopilot. In this paper the component of the ocean current acting in the sway direction is chosen as the integrated error signal, instead of the absolute sway velocity. It is shown that this separates the underactuated sway dynamics from the closed loop guidance dynamics. This simplifies the control system. Moreover, the sway subsystem is shown to be input-to-state stable (ISS). Again, the closed loop system reveals multiple stable/unstable equilibrium points, corresponding to the counter-current/co-current directions, respectively. The sign of a gain parameter selects which of the two courses is the stable one. Compared to Caharija et al. (2013), the complete cascaded closed loop system is considered and uniform semiglobal asymptotic stability (USAS), in addition to uniform local exponential stability (ULES), is shown. The proposed solution performs counter-current or co-current guidance in presence of constant and irrotational ocean currents, acting in any direction of the inertial frame. Lyapunov theory (Khalil, 2000) and nonlinear control theory of cascades (Grøtli et al., 2008; Chaillet and Loría, 2006, 2008) are used in the proof.

The paper is organized as follows: Section 2 presents the control plant model of the vehicle, Section 3 identifies the control objective and Section 4 presents the strategy that solves the control task. The main result is stated in Section 5 and proven in Section 6. Simulation results and conclusions are given in Section 7 and Section 8, respectively.

2. THE VEHICLE MODEL

2.1 Model Assumptions

Assumption 1. The motion of the vehicle is described in 3 degrees of freedom, that is surge, sway and yaw.

Assumption 2. The vehicle is port-starboard symmetric.

Assumption 3. The body-fixed coordinate frame b is considered located at a point $(x_g^*, 0)$ from the vehicle's center of gravity (CG) along the center-line of the vessel, where x_g^* is to be defined later.

Remark 1. The body-fixed coordinate system can always be translated to the required location x_g^* Fossen (2011).

Assumption 4. Damping is considered linear.

Remark 2. Nonlinear damping is not considered in order to reduce the complexity of the controllers. However, the passive nature of the non-linear hydrodynamic damping forces should enhance the directional stability of the vessel.

Assumption 5. The ocean current in the inertial frame i, $\boldsymbol{V}_c \triangleq [V_x, V_y]^T$, is constant, irrotational and bounded. Hence, there exists a constant $V_{\max} > 0$ such that $V_{\max} > \sqrt{V_x^2 + V_y^2}$.

2.2 The Control Model

The state of the vessel is given by the vector $[\boldsymbol{p}^T, \boldsymbol{\nu}^T]^T$ where $\boldsymbol{p} \triangleq [x, y, \psi]^T$ describes the position and the orientation of the vehicle with respect to the inertial frame i. The vector $\boldsymbol{\nu} \triangleq [u, v, r]^T$ contains the linear and angular velocities of the vessel defined in the body-fixed frame b, where u is the surge velocity, v is the sway velocity and r is the yaw rate. The ocean current velocity in the body frame b, $\boldsymbol{\nu}_c \triangleq [u_c, v_c, 0]^T$, is obtained from $\boldsymbol{\nu}_c = \boldsymbol{R}^T(\psi)[V_x, V_y, 0]^T$ where $\boldsymbol{R}(\psi)$ is the rotation matrix from b to i. $\boldsymbol{R}(\psi)$ is defined in (4) using the xyz convention. The ocean current is constant and irrotational in i, i.e. $\dot{\boldsymbol{V}}_c = \boldsymbol{0}$ and therefore:

$$\dot{\boldsymbol{\nu}}_c = [r v_c, -r u_c, 0]^T. \tag{1}$$

In navigation problems involving ocean currents it is useful to introduce the relative velocity: $\boldsymbol{\nu}_r \triangleq \boldsymbol{\nu} - \boldsymbol{\nu}_c = [u_r, v_r, r]^T$. The vector $\boldsymbol{\nu}_r$ is defined in b, where u_r is the relative surge velocity and v_r is the relative sway velocity.

In this paper, the class of marine vehicles described by the following 3-DOF maneuvering model are considered Fossen (2011):

$$\dot{\boldsymbol{p}} = \boldsymbol{R}(\psi)\boldsymbol{\nu}_r + [V_x, V_y, 0]^T, \tag{2}$$

$$\boldsymbol{M}\dot{\boldsymbol{\nu}}_r + \boldsymbol{C}(\boldsymbol{\nu}_r)\boldsymbol{\nu}_r + \boldsymbol{D}\boldsymbol{\nu}_r = \boldsymbol{B}\boldsymbol{f}. \tag{3}$$

Remark 3. It is shown in Fossen (2011) that since the current is constant and irrotational in i, the 3-DOF maneuvering model of the vehicle can be formulated as (2-3).

The vector $\boldsymbol{f} \triangleq [T_u, T_r]^T$ is the control input vector, containing the surge thrust T_u and the rudder angle T_r. Notice that the model (3) is underactuated in its configuration space. The matrix $\boldsymbol{M} = \boldsymbol{M}^T > 0$ is the mass and inertia matrix, and includes hydrodynamic added mass. The matrix $\boldsymbol{C}$ is the Coriolis and centripetal matrix, $\boldsymbol{D} > 0$ is the hydrodynamic damping matrix and $\boldsymbol{B} \in \mathbb{R}^{3\times 2}$ is the actuator configuration matrix. For manoeuvring control purposes, the matrices $\boldsymbol{M}$, $\boldsymbol{D}$ and $\boldsymbol{B}$ can be considered as having the following structure:

$$\boldsymbol{R}(\psi) \triangleq \begin{bmatrix} \cos(\psi) & -\sin(\psi) & 0 \\ \sin(\psi) & \cos(\psi) & 0 \\ 0 & 0 & 1 \end{bmatrix}, \quad \boldsymbol{M} \triangleq \begin{bmatrix} m_{11} & 0 & 0 \\ 0 & m_{22} & m_{23} \\ 0 & m_{23} & m_{33} \end{bmatrix}, \tag{4}$$

$$\boldsymbol{D} \triangleq \begin{bmatrix} d_{11} & 0 & 0 \\ 0 & d_{22} & d_{23} \\ 0 & d_{32} & d_{33} \end{bmatrix}, \quad \boldsymbol{B} \triangleq \begin{bmatrix} b_{11} & 0 \\ 0 & b_{22} \\ 0 & b_{32} \end{bmatrix}. \tag{5}$$

The particular structure of $\boldsymbol{M}$ and $\boldsymbol{D}$ is justified by Assumptions 1-4. The actuator configuration matrix $\boldsymbol{B}$ has full column rank and maps the control inputs T_u and T_r into forces and moments acting on the vessel. The Coriolis and centripetal matrix $\boldsymbol{C}$ is obtained from $\boldsymbol{M}$ as shown in Fossen (2011):

$$\boldsymbol{C}(\boldsymbol{\nu}_r) \triangleq \begin{bmatrix} 0 & 0 & -m_{22}v_r - m_{23}r \\ 0 & 0 & m_{11}u_r \\ m_{22}v_r + m_{23}r & -m_{11}u_r & 0 \end{bmatrix}. \tag{6}$$

Finally, x_g^* from Assumption 3 is chosen so that $\boldsymbol{M}^{-1}\boldsymbol{B}\boldsymbol{f} = [\tau_u, 0, \tau_r]^T$. The point $(x_g^*, 0)$ exists for all port-starboard symmetric vehicles (Caharija et al., 2012b).

2.3 The Model in Component Form

To solve nonlinear underactuated control design problems it is useful to expand (2-3) into:

$$\dot{x} = u_r \cos(\psi) - v_r \sin(\psi) + V_x, \quad (7a)$$
$$\dot{y} = u_r \sin(\psi) + v_r \cos(\psi) + V_y, \quad (7b)$$
$$\dot{\psi} = r, \quad (7c)$$
$$\dot{u}_r = F_{u_r}(v_r, r) - (d_{11}/m_{11})u_r + \tau_u, \quad (7d)$$
$$\dot{v}_r = X(u_r)r + Y(u_r)v_r, \quad (7e)$$
$$\dot{r} = F_r(u_r, v_r, r) + \tau_r. \quad (7f)$$

The expressions for $F_r(u_r, v_r, r)$, $F_{u_r}(v_r, r)$, $X(u_r)$ and $Y(u_r)$ are given in Appendix B. Notice that the functions $Y(u_r)$ and $X(u_r)$ are bounded for bounded arguments and thus the following notation is used:

$$X^{\max} \triangleq \max_{\Omega} |X(u_r)|, \quad (8)$$

where $\Omega \triangleq \{-V_{\max} \le u_r \le U_{rd} + V_{\max}\}$ and the following assumption is introduced:

Assumption 6. The function $Y(u_r)$ satisfies

$$Y(u_r) \le -Y^{\min} < 0, \quad \forall u_r \in \Omega.$$

Remark 4. Assumption 6 is justified by a contradiction: $Y(u_r) \ge 0$ would imply a nominally unstable vehicle in sway which is not the case for commercial vessels by design. Furthermore, notice that no bounds are implied on u_r. The constant $U_{rd} > 0$ is a design parameter and is defined in Section 3.

3. THE CONTROL OBJECTIVE

This section formalizes the control problem solved in this paper: the control system should make the vessel turn against the current, or follow the current, in the complementary case. In addition, the vehicle should also maintain a desired constant surge relative velocity $U_{rd} > 0$. The ocean current is considered constant and unknown. The case of a marine vehicle moving at constant speed and holding a constant course ψ_c, in presence of ocean currents, should be considered first to properly define the control objectives. This case has been addressed in Børhaug et al. (2008), Caharija et al. (2012a) and Caharija et al. (2012c), where it has been proven that the relative sway velocity of the vessel, v_r, decays exponentially to zero due to Assumption 6. Furthermore it can be seen that the current component acting in the sway direction v_c becomes $v_c \to v_{c,ss} \triangleq -V_x \sin(\psi_c) + V_y \cos(\psi_c)$, exponentially. Therefore, in presence of constant irrotational ocean current, $v_r \to 0$ and $v_c \to v_{c,ss}$, at steady state.

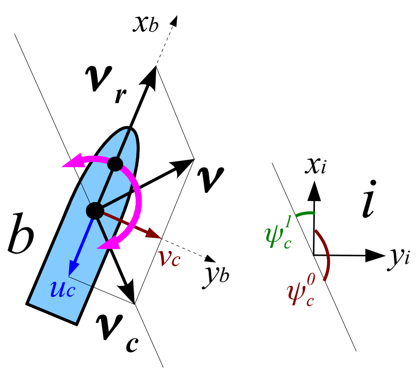

Fig. 1. The vehicle has to align its relative velocity vector $\boldsymbol{\nu}_r$ with the current vector $\boldsymbol{\nu}_c$ to perform counter-current or co-current guidance.

To achieve counter-current guidance as well as co-current guidance, the vessel is required to align its relative velocity vector $\boldsymbol{\nu}_r$ with the current velocity vector $\boldsymbol{\nu}_c$, as shown in Figure 1. At steady state, when the two vectors are parallel, the current vector $\boldsymbol{\nu}_c$ has clearly its sway component $v_{c,ss} = 0$. It is trivial to show that $v_{c,ss} = 0$ if and only if the vessel is pointing against the current or going with the current, i.e. if and only if $\psi_c = \mathrm{atan2}(V_y, V_x) + k\pi,\ k \in \mathbb{Z}$. Hence, the objectives the control system should pursue can be formalized as follows:

$$\lim_{t\to\infty} v_c(t) = 0, \quad (9)$$
$$\lim_{t\to\infty} \psi(t) = \mathrm{atan2}(V_y, V_x) + k\pi, \quad k \in \{0, 1\}, \quad (10)$$
$$\lim_{t\to\infty} u_r(t) = U_{rd}, \quad (11)$$

where $k = 0$ identifies the co-current guidance and $k = 1$ identifies the counter-current guidance. Finally, the following assumption allows the vessel to move against sea currents acting in any directions of the plane:

Assumption 7. The propulsion system is rated with power and thrust capacity such that U_{rd} satisfies $U_{rd} > V_{\max}$.

Remark 5. For most marine vehicles Assumption 7 is easy to meet since their propulsion systems are typically designed to give more than $2 - 3$ [m/s] of relative speed U_{rd}. The ocean current has usually an intensity of less than 1 [m/s].

Remark 6. Notice that Assumption 7 is strictly necessary for the vessel to be able to move against the current.

Remark 7. It is trivial to show that the absolute sway velocity $v \to 0$ when the control objectives (9-10) are achieved since $v = v_r + v_c$. This property is exploited in Caharija et al. (2013) to search for the current direction. In this paper the signal v_c represent the error signal instead.

4. THE CONTROL SYSTEM

A control system that solves the control problem defined in Section 3 is presented. First the guidance system is introduced, and then the surge and yaw controllers are added in a cascaded configuration.

4.1 The Guidance Strategy

The following heading reference is proposed to achieve counter-current guidance, or alternatively co-current guidance:

$$\psi_G \triangleq -\sigma v_{\mathrm{int}}, \quad \sigma \ne 0, \quad (12a)$$
$$\dot{v}_{\mathrm{int}} = v_c, \quad (12b)$$

where $\sigma > 0$ makes the vehicle turn against the flow and $\sigma < 0$ makes the vehicle follow the flow. The integral effect (12b) forces the vessel to search for the two directions having zero current component in the sway direction v_c at steady state, while the sign of the gain σ defines whether the counter-current course or the co-current course is the stable equilibrium point of the closed loop system. This paper shows how the simple and intuitive guidance system (12) performs counter-current guidance, or co-current guidance, with stronger stability properties than Caharija et al. (2013). Notice that alternative integral laws, such as the one introduced in Børhaug et al. (2008), can be used to improve the performance of (12).

Remark 8. The error signal in (12b) is the current component acting in the sway direction. This component can be measured or estimated using DVL devices or other sensor fusion techniques (Morgado et al., 2011; Fossen, 2011).

4.2 Surge and Yaw Controllers

According to (11), $u_r(t)$ should follow the desired value $u_{rd}(t) \triangleq U_{rd} > 0$. To this end the following controller is used:

$$\tau_u = -F_{u_r}(v_r, r) + \frac{d_{11}}{m_{11}} u_{rd} + \dot{u}_{rd} - k_{u_r}(u_r - u_{rd}). \quad (13)$$

The gain $k_{u_r} > 0$ is constant. The controller (13) is a feedback linearizing P-controller and guarantees exponential tracking of $u_{rd}(t)$ (cf. Eq. (15) below). Note that part of the damping is not canceled in order to guarantee some robustness with respect to model uncertainties. The following controller can be used to track the desired yaw angle $\psi_d \triangleq \psi_G$:

$$\tau_r = -F_r(u_r, v_r, r) + \ddot{\psi}_d - k_\psi(\psi - \psi_d) - k_r(\dot{\psi} - \dot{\psi}_d), \quad (14)$$

where $k_\psi, k_r > 0$ are constant gains. The controller (14) is a feedback linearizing PD controller and makes sure that ψ and r exponentially track ψ_d and $\dot{\psi}_d$ (cf. Eq (16) below).

Remark 9. Notice that $\dot{\psi}_d$ and $\ddot{\psi}_d$ are well defined if $\psi_d \triangleq \psi_G$ since (1) is a consequence of Assumption 5.

5. MAIN RESULT

This section presents the conditions under which the proposed control system achieves the objectives (9-11). The counter-current guidance case ($\sigma > 0$) is considered only. However, the same derivations and conclusions can be drawn for the co-current case ($\sigma < 0$).

Theorem 1. Given an underactuated marine vehicle described by the dynamical system (7). If Assumptions 1-7 hold, the controllers (13-14), with $k_{u_r}, k_\psi, k_r > 0$, $u_{rd} \triangleq U_{rd}$ and $\psi_d \triangleq \psi_G$, guarantee achievement of the control objectives (9-11) with USAS and ULES properties. The USAS properties hold on the parameter set $\Theta \triangleq \{\sigma > 0\}$.

Proof. The proof of Theorem 1 is given in Section 6. □

6. PROOF OF THEOREM 1

The actuated surge and yaw dynamics of the vehicle are considered first. The closed loop surge subsystem is obtained combining (7d) with (13) and given $\tilde{u}_r \triangleq u_r - U_{rd}$, the $\tilde{u}_r$ dynamics become:

$$\dot{\tilde{u}}_r = -\left(\frac{d_{11}}{m_{11}} + k_{u_r}\right)\tilde{u}_r, \quad (15)$$

where $d_{11}, m_{11}, k_{u_r} > 0$. The $\tilde{u}_r$ subsystem is clearly uniformly globally exponentially stable (UGES). Therefore, the control goal (11) is achieved exponentially in any ball of initial conditions.

The yaw ψ, r subsystem is obtained from (7c) and (7f) in closed loop configuration with (14). Given the error variables $\tilde{\psi} \triangleq \psi - \psi_d$ and $\tilde{r} \triangleq r - \dot{\psi}_d$, the dynamics of $\tilde{\psi}$ and $\tilde{r}$ are:

$$\dot{\boldsymbol{\xi}} = \begin{bmatrix} 0 & 1 \\ -k_\psi & -k_r \end{bmatrix} \boldsymbol{\xi} \triangleq \boldsymbol{\Sigma\xi}, \quad (16)$$

where $\boldsymbol{\xi} \triangleq [\tilde{\psi}, \tilde{r}]^T$. The system (16) is linear and time-invariant. Furthermore, since the gains k_ψ, k_r are strictly positive, the system matrix $\boldsymbol{\Sigma}$ is Hurwitz and hence the origin $\boldsymbol{\xi} = \boldsymbol{0}$ is UGES.

The guidance system (12) is considered next. Since $\boldsymbol{\nu}_c = \boldsymbol{R}^T(\psi)\boldsymbol{V}_c$ (see Section 2) and $\tilde{\psi} \triangleq \psi - \psi_d$, the integrator (12b) can be written as:

$$\dot{v}_{\text{int}} = -V_x \sin(\psi_d + \tilde{\psi}) + V_y \cos(\psi_d + \tilde{\psi}), \quad (17)$$

where $\psi_d = -\sigma v_{\text{int}}$. The interconnected dynamics of v_{int} are given combining (17) with (16):

$$\begin{aligned} \dot{v}_{\text{int}} &= V_x \sin(\sigma v_{\text{int}}) + V_y \cos(\sigma v_{\text{int}}) \\ &\quad + \boldsymbol{H}_v(v_{\text{int}}, \boldsymbol{\xi})\boldsymbol{\xi}, \end{aligned} \quad (18a)$$

$$\dot{\boldsymbol{\xi}} = \boldsymbol{\Sigma\xi}, \quad (18b)$$

where $\boldsymbol{H}_v(v_{\text{int}}, \boldsymbol{\xi}) \triangleq [h_{v_{\text{int}}}(v_{\text{int}}, \tilde{\psi}),\ 0]$ and the function $h_{v_{\text{int}}}(v_{\text{int}}, \tilde{\psi})$ is given in Appendix B. The system (18) is a cascaded system where the linear UGES system (18b) perturbs the dynamics (18a) through the interconnection term $\boldsymbol{H}_v$.

Remark 10. Compared to Caharija et al. (2013), the relative sway velocity v_r does not show up in (18). This is due to the choice of v_c instead of v as the error signal in (12). Complexity of the closed loop stability analysis is therefore reduced.

Analyzing (18) at equilibrium shows that $\boldsymbol{\xi}^{\text{eq}} = \boldsymbol{0}$ and:

$$V_x \sin(\sigma v^{\text{eq}}_{\text{int}}) + V_y \cos(\sigma v^{\text{eq}}_{\text{int}}) = 0, \quad (19)$$

therefore:

$$v^{\text{eq}}_{\text{int},k} = -(1/\sigma)\left[\text{atan2}\left(V_y, V_x\right) + k\pi\right], \quad k \in \mathbb{Z}. \quad (20)$$

The system (18) has multiple equilibrium points that identify two physical directions: the counter-current direction and the co-current direction. This is clearly seen if the course held by the ship at equilibrium is calculated:

$$\psi^{\text{eq}}_k = \text{atan2}\left(V_y, V_x\right) + k\pi, \quad k \in \mathbb{Z}, \quad (21)$$

where the equilibrium points with $k = 1 + 2n, n \in \mathbb{Z}$ correspond to the counter-current direction, while the equilibrium points identified by $k = 2n, n \in \mathbb{Z}$ correspond to the co-current direction. In particular, the equilibrium point with $k = 1$ that corresponds to the counter-current course, $v^{\text{eq}}_{\text{int},1}$, is considered.

Remark 11. The equilibrium point having $k = 1$ is equivalent to all the counter-current equilibrium points identified by $k = 1 + 2n, n \in \mathbb{Z}$, hence their analysis is identical.

The variable $e \triangleq v_{\text{int}} - v^{\text{eq}}_{\text{int},1}$ is introduced to move the equilibrium point to the origin. This is in fact a rotation of the inertial frame i for an angle ψ^{eq}_1. The cascaded system (18) can be then rewritten in the following form:

$$\dot{e} = -V_c \sin(\sigma e) + \boldsymbol{H}_e(e, \boldsymbol{\xi})\boldsymbol{\xi}, \quad (22a)$$

$$\dot{\boldsymbol{\xi}} = \boldsymbol{\Sigma\xi}, \quad (22b)$$

where $V_c > 0$ is the magnitude of the ocean current, $V_c \triangleq \sqrt{V_x^2 + V_y^2}$, and $\boldsymbol{H}_e \triangleq [h_e(e, \tilde{\psi}),\ 0]$. The function $h_e(e, \tilde{\psi})$ is given in Appendix B. The following nominal system is analyzed first to assess the stability properties of the cascade (22):

$$\dot{e} = -V_c \sin(\sigma e). \quad (23)$$

The following lemma states uniform semiglobal exponential stability (USES) for (23).

Lemma 2. Under the conditions of Theorem 1, the system (23) is USES.

Proof. Consider the quadratic Lyapunov function candidate $V_1 \triangleq (1/2)e^2$. In any ball $\mathcal{B}_{1/\sigma} \triangleq \{|e| \leq 1/\sigma\}$, the time-derivative of V_1 satisfies the following bound:

$$\dot{V}_1 = -V_c e \sin(\sigma e) \leq -V_c \sigma \frac{e^2}{2} = -V_c \sigma V_1. \tag{24}$$

Notice that the tuning parameter $\sigma > 0$ can be chosen arbitrarily small and that V_1 is independent of σ. This shows exponential stability on a domain of attraction that can be made arbitrarily large by picking σ small enough. Therefore, according to Theorem 2 in Grøtli et al. (2008), it is possible to conclude uniform semiglobal exponential stability on the parameter set $\Theta = \{\sigma > 0\}$ for the nominal system (23). □

Remark 12. Notice that USES implies USAS. Precise definitions of the USES and USAS properties are given in Grøtli et al. (2008) (Definition 2) and in Chaillet and Loría (2006) (Definition 2.2), respectively.

Remark 13. Even though the equilibria of (22) are multiple, they all can be separated by an arbitrarily large distance by picking $\sigma > 0$ small enough. This explains intuitively why the stability properities of (23) hold semiglobally.

The next lemma shows uniform boundedness (UB) for (22).

Lemma 3. Under the conditions of Theorem 1, the solutions of (22) are uniformly and ultimately bounded.

Proof. The proof of Lemma 3 is given in Appendix A. □

Lemma 4 proves USAS stability for the cascade (22).

Lemma 4. Under the conditions of Theorem 1, the cascaded system (22) is USAS.

Proof. Theorem 18 from Chaillet and Loría (2008) is applied to show USAS stability of the cascade (22). In particular, Assumptions 16, 19, 20 and 21 from Chaillet and Loría (2008) need to be satisfied:

- [*Interconnection*] It can be shown that the interconnection term in (22a) satisfies the following bound and hence Assumption 16 of Chaillet and Loría (2008) is satisfied:
$$\boldsymbol{H}_e(e, \boldsymbol{\xi})\boldsymbol{\xi} = \tilde{\psi} h_e(e, \tilde{\psi}) < 2V_{\max}|\tilde{\psi}|. \tag{25}$$
- [*USAS of* (22b)] As shown at the beginning of this section, the perturbing system is UGES and thus Assumption 19 of Chaillet and Loría (2008) is trivially satisfied.
- [*USAS of* (23)] Lemma 2 shows USES on $\sigma > 0$ for the nominal system (23). It is straightforward to show that Assumption 20 of Chaillet and Loría (2008) is fulfilled since V_1 is independent of σ.
- [*UB of* (22)] Lemma 3 proves uniform ultimate boundedness of the solutions of (22). The bounds (A.7) and (A.8) are linearly dependent on $1/\sigma$, and hence it can be seen that Assumption 21 of Chaillet and Loría (2008) is satisfied as well.

This, according to Theorem 18 of Chaillet and Loría (2008), concludes USAS on the parameter set $\Theta = \{\sigma > 0\}$ of the cascaded system (22). □

In addition to USAS, uniform local exponential stability (ULES) of (22) is shown by linearizations:

$$\dot{\boldsymbol{\chi}} = \begin{bmatrix} -\sigma V_c & V_c & 0 \\ 0 & 0 & 1 \\ 0 & -k_\psi & -k_r \end{bmatrix} \boldsymbol{\chi} \triangleq \boldsymbol{A}\boldsymbol{\chi}, \tag{26}$$

where $\boldsymbol{\chi} \triangleq [e, \tilde{\psi}, \tilde{r}]^T$. The matrix $\boldsymbol{A}$ is Hurwitz and therfore the origin is of (22) is also ULES. Hence, following Remark 11, all the counter-current equilibrium points ($k = 1 + 2n, n \in \mathbb{Z}$) have USAS and ULES properties. Similarly, linearization shows instability of the equilibrium points identifying the co-current direction ($k = 2n, n \in \mathbb{Z}$). Finally, ISS for the sway dynamics (7e) is shown:

Lemma 5. Under the conditions of Theorem 1, the sway subsystem (7e) is ISS.

Proof. The underactuated sway subsystem (7e) can be rewritten using $r = \dot{\psi}_d + \tilde{r}$:

$$\dot{v}_r = Y(u_r)v_r + X(u_r)f(\boldsymbol{\chi}), \tag{27}$$

where:

$$f(\boldsymbol{\chi}) \triangleq \sigma V_c \sin(\sigma e) - \sigma \tilde{\psi} h_e(e, \tilde{\psi}) + \tilde{r}, \tag{28}$$

and it can be shown that:

$$|f(\boldsymbol{\chi})| \leq g(||\boldsymbol{\chi}||) \triangleq \kappa(|e| + |\tilde{\psi}| + |\tilde{r}|), \tag{29}$$

for some $\kappa > 0$. Notice that $\boldsymbol{\chi}(t)$ perturbs the sway subsystem and that $f(\mathbf{0}) = 0$. The unforced sway subsystem is $\dot{v}_r = Y(u_r)v_r$. Applying (29) and Assumption 6 to the time derivative of the quadratic function $V_2 \triangleq (1/2)v_r^2$ yields the following bound:

$$\begin{aligned} \dot{V}_2 &= Y(u_r)v_r^2 + X(u_r)f(\boldsymbol{\chi})v_r \leq \\ &\leq -Y^{\min}v_r^2 + X^{\max}g(||\boldsymbol{\chi}||)|v_r|. \end{aligned} \tag{30}$$

Given $0 < \theta < 1$, (30) becomes:

$$\dot{V}_2 \leq -(1-\theta)Y^{\min}v_r^2, \ \forall |v_r| \geq \frac{1}{\theta}\frac{X^{\max}}{Y^{\min}} g(||\boldsymbol{\chi}||) > 0. \tag{31}$$

Hence, following Theorem 4.19 in Khalil (2000), the sway subsystem (7e) is ISS with respect to $\boldsymbol{\chi}$. □

Remark 14. The use of Assumption 6 in the proof of Lemma 5 is justified by the fact that u_r is bounded, as clearly shown at the beginning of this section. See Børhaug et al. (2008); Caharija et al. (2012c) for similar arguments.

To conclude, the controllers (13-14) guarantee USAS on the parameter set $\Theta = \{\sigma > 0\}$ as well as ULES of the counter-current equilibrium points ($k = 1 + 2n, n \to \mathbb{Z}$), of the closed loop system (22). Hence, for any ball of initial conditions $\boldsymbol{\chi}_o$ there exists a small enough $\sigma > 0$ such that the objectives (9-11) are achieved asymptotically. Locally, (9-11) are achieved exponentially for all $\sigma > 0$.

7. SIMULATIONS

In this section results from numerical simulations are presented. The developed guidance law is applied to an underactuated supply vessel. The model parameters of the ship are given in Fredriksen and Pettersen (2004) and the objective is to make the vessel move against the sea current or, complementary, to follow the sea current. The ship should also hold a desired surge relative speed $U_{rd} = 2$ [m/s]. Notice that the guidance law sets the heading of the vessel only, while its position is unconstrained. The intensity of the current is $|\boldsymbol{V}_c| = 1/\sqrt{2}$ [m/s] and its direction is randomly generated. In this case, its components are

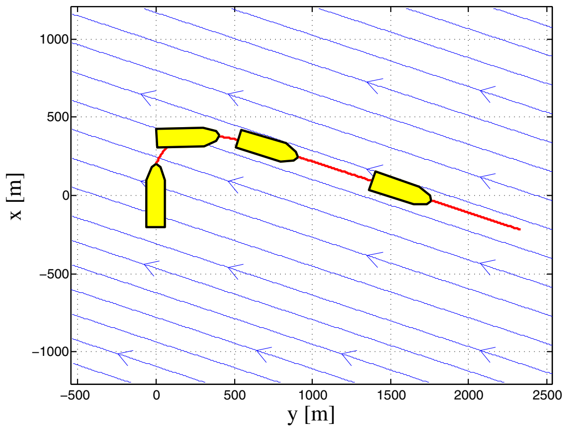

Fig. 2. Counter-current guidance of an underactuated supply ship ($\sigma = 0.01$). The ship turns and moves against the flow since, in this case, $U_{rd} > V_{\max}$.

$V_x = 0.2209$ [m/s] and $V_y = -0.6717$ [m/s], giving a direction of $-71.8°$. Thus, Assumptions 5 and 7 are fulfilled with $V_{\max} = 0.71$ [m/s]. Furthermore, it can be verified that Assumption 6 is satisfied with $Y^{\min} = 0.3494$ [s^{-1}] and $X^{\max} = 1.5340$ [m/s].

The chosen values for the gain σ in the counter-current case and in the co-current case are 0.01 [m^{-1}] and -0.01 [m^{-1}], respectively. Choosing too high values for σ may induce chattering due to saturation in the magnitude and the turning rate of the rudder actuators. The linearized system (26) shows that the convergence rate of the guidance law is in first approximation dependent on the constant σV_c. Given that $V_c = 1/\sqrt{2}$ [m/s] and $|\sigma| = 0.01$ [m^{-1}], this gives a time constant of 141[s]. In particular, the restoring term $V_c \sin(\sigma e)$ is strongest at the origin, thus the guidance dynamics are faster close to the stable equilibrium point. The internal controllers (13-14) are implemented with the following gains: $k_{u_r} = 0.1$, $k_\psi = 0.04$ and $k_r = 0.9$. Hence, the $\tilde{u}_r$ first order closed loop system (15) has a time constant of 8.8 [s] while the $\tilde{\psi}$ second order closed loop system (16) is overdamped with $\omega_0 = 0.2$ [rad/s].

The ship is initially located at the origin of the inertial frame and holds zero relative velocity. Its surge axis is parallel to the x axis of the inertial frame. Figures 2 and 4 show how counter-current and co-current guidance are successfully achieved. Notice that the current is acting in the $-71.8°$ direction and that the guidance law correctly identifies the counter-current course as well as the co-current course (Figures 3 and 5). The practical implementability of the counter-current/co-current guidance can be assessed by analyzing the rudder angle of the vessel from Figures 3 and 5. Notice that in the simulations saturation is taken into account for both the rudder and the propeller. The maximum rudder angle is 35° and the maximum rudder turning rate is 10 [°/s]. The maximum propeller force is 1600 [kN]. Figures 3 and 5 show that the controller moves the rudder smoothly without sharp variations and does not reach saturation. This illustrates that the proposed guidance is implementable as long as reliable measurements of the v_c current component are available.

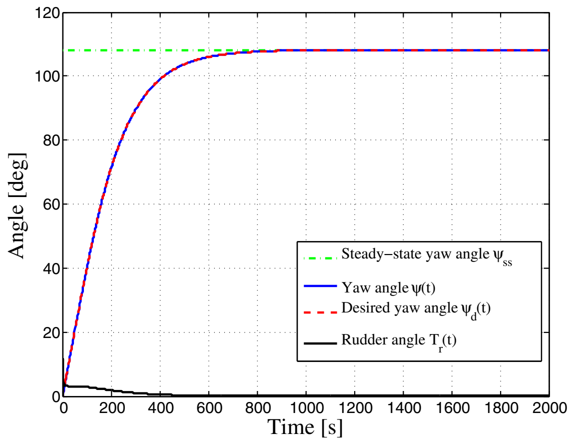

Fig. 3. Yaw angle $\psi(t)$ of the ship in counter-current guidance mode ($\sigma = 0.01$). Notice that the steady state yaw angle is $\psi_{ss} = 108.2°$ which is exactly the counter current direction (The current direction is $-71.8°$).

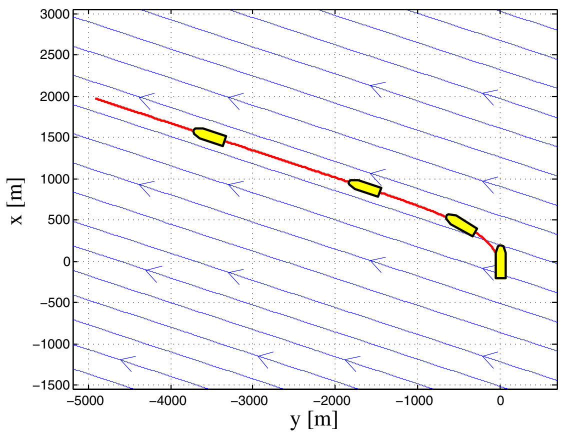

Fig. 4. Co-current guidance of an underactuated supply ship ($\sigma = -0.01$). The ship turns with the current and follows the flow.

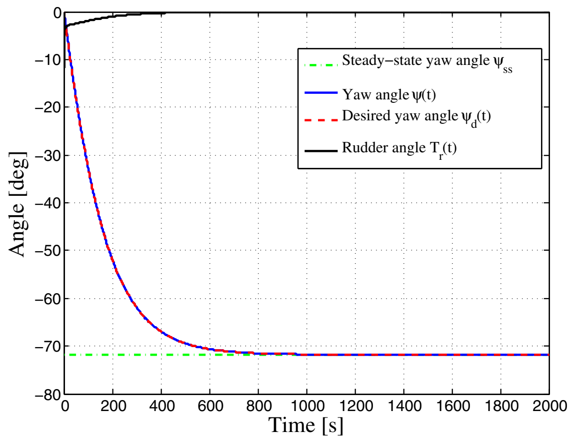

Fig. 5. Yaw angle $\psi(t)$ of the ship in co-current guidance mode ($\sigma = -0.01$). Notice that the steady state yaw angle is $\psi_{ss} = -71.8°$ which is exactly the current direction.

8. CONCLUSIONS

In this paper an improved control strategy for counter-current and co-current guidance of underactuated unmanned marine vehicles has been presented. In particular, USES and ULES stability properties are shown for the complete multiple-equilibria closed loop system. The control system is based on an integral guidance law where the current component acting in the sway direction represents the error signal. As a result, the vessel determines the two possible directions having zero absolute sway velocity: the counter-current course and the co-current course. The two directions represent a set of stable equilibrium points and a set of unstable equilibrium points. The sign of the gain σ defines whether the vehicle converges to the counter-current direction or to the co-current direction. Numerical simulations support the theoretical results.

ACKNOWLEDGMENTS

The authors are very grateful to Antoine Chaillet and to Antonio Loria for their help in the proof of Theorem 1.

REFERENCES

Aguiar, A. and Pascoal, A.M. (1997). Modeling and control of an autonomous underwater shuttle for the transport of benthic laboratories. In *Proc. of MTS/IEEE Conference OCEANS '97*, 888–895.

Antonelli, G. (2007). On the use of adaptive/integral actions for six-degrees-of-freedom control of autonomous underwater vehicles. *IEEE Journal of Oceanic Engineering*, 32(2), 300–312.

Batista, P., Silvestre, C., and Oliveira, P. (2012). GES integrated LBL/USBL navigation system for underwater vehicles. In *Proc. of the IEEE 51st Conference on Decision and Control*, 6609–6614.

Breivik, M. and Fossen, T.I. (2009). *Guidance Laws for Autonomous Underwater Vehicles*, chapter 4, 51–76. A. V. Inzartsev, IN-TECH Education and Publishing.

Børhaug, E., Pavlov, A., and Pettersen, K.Y. (2008). Integral LOS control for path following of underactuated marine surface vessels in the presence of constant ocean currents. In *Proc. of the 47th IEEE Conference on Decision and Control*, 4984–4991.

Caharija, W., Candeloro, M., Pettersen, K.Y., and Sørensen, A.J. (2012a). Relative velocity control and integral LOS for path following of underactuated surface vessels. In *Proc. of the 9th IFAC Conference on Manoeuvring and Control of Marine Craft*.

Caharija, W., Pettersen, K.Y., and Gravdahl, J.T. (2013). Counter-current and co-current guidance of underactuated unmanned marine vehicles. In *Proc. of the 8th IFAC Symposium on Intelligent Autonomous Vehicles*, 184–191.

Caharija, W., Pettersen, K.Y., Gravdahl, J.T., and Børhaug, E. (2012b). Integral LOS guidance for horizontal path following of underactuated autonomous underwater vehicles in the presence of vertical ocean currents. In *Proc. of American Control Conf.*, 5427–5434.

Caharija, W., Pettersen, K.Y., Gravdahl, J.T., and Børhaug, E. (2012c). Path following of underactuated autonomous underwater vehicles in the presence of ocean currents. In *Proc. of the 51st IEEE Conference on Decision and Control*, 528–535.

Chaillet, A. and Loría, A. (2006). Necessary and sufficient conditions for uniform semiglobal practical asymptotic stability: Application to cascaded systems. *Automatica*, 42(11), 1899–1906.

Chaillet, A. and Loría, A. (2008). Uniform semiglobal practical asymptotic stability for non-autonomous cascaded systems and applications. *Automatica*, 44(2), 337–347.

Do, K.D., Pan, J., and Jiang, Z.P. (2004). Robust and adaptive path following for underactuated autonomous underwater vehicles. *Ocean Engineering*, 31, 1967–1997.

Encarnação, P., Pascoal, A.M., and Arcak, M. (2000). Path following for marine vehicles in the presence of unknown currents. In *Proc. of the 6th IFAC International Symposium on Robot Control*, 469–474.

Fossen, T.I. (2011). *Handbook of Marine Craft Hydrodynamics and Motion Control*. John Wiley & Sons, Inc., Hoboken, NJ.

Fossen, T.I. and Strand, J.P. (2001). Nonlinear passive weather optimal positioning control (WOPC) system for ships and rigs: experimental results. *Automatica*, 37(5), 701–715.

Fredriksen, E. and Pettersen, K.Y. (2004). Global κ-exponential way-point manoeuvering of ships. In *Proc. of the 43rd IEEE Conference on Decision and Control*, 5360–5367.

Grøtli, E.I., Chaillet, A., and Gravdahl, J.T. (2008). Output control of spacecraft in leader follower formation. In *Proc. of the 47th IEEE Conference on Decision and Control*, 1030–1035.

Indiveri, G., Creti, S., and Zizzari, A.A. (2012). A proof of concept for the guidance of 3D underactuated vehicles subject to constant unknow disturbances. In *Proc. of the 9th IFAC Conference on Manoeuvring and Control of Marine Crafts*.

Jouffroy, J., Zhou, Q., and Zielinski, O. (2011). Towards selective tidal-stream transport for lagrangian profilers. In *Proc. of MTS/IEEE Conference OCEANS '11*, 1–6.

Khalil, H. (2000). *Nonlinear Systems*. Pearson Education International inc., Upper Saddle River, NJ, USA, 3rd ed. edition.

Kjerstad, Ø.K. and Breivik, M. (2010). Weather optimal positioning control for marine surface vessels. In *Proc. of the 8th IFAC Conference on Control Applications in Marine Systems*.

Morgado, M., Batista, P., Oliveira, P., and Silvestre, C. (2011). Position USBL/DVL sensor-based navigation filter in the presence of unknown ocean currents. *Automatica*, 47(12), 2604–2614.

Refsnes, J.E., Sørensen, A.J., and Pettersen, K.Y. (2007). Output feedback control of slender body underwater vehicles with current estimation. *International Journal of Control*, 80(7), 1136–1150.

Smith, R.N., Schwager, M., Smith, S.L., Jones, B.H., Rus, D., and Sukhatme, G.S. (2011). Persistent ocean monitoring with underwater gliders: Adapting sampling resolution. *Journal of Field Robotics*, 28(5), 714–741.

Yoerger, D.R., Jakuba, M., Bradley, A.M., and Bingham, B. (2007). Techniques for deep sea near bottom survey using an autonomous underwater vehicle. *The International Journal of Robotics Research*, 26(1), 41–54.

Appendix A. PROOF OF LEMMA 3

In the following discussion the notation $\lambda_m(\boldsymbol{A})$ and $\lambda_M(\boldsymbol{A})$ is introduced to denote the minimum and maximum eigenvalue, respectively, of a matrix $\boldsymbol{A}$. The Euclidean norm $\|\cdot\| \triangleq \|\cdot\|_2$ is used.

Given the positive definite quadratic function $V_3(\boldsymbol{\chi})$:

$$V_3 \triangleq \boldsymbol{\chi}^T \boldsymbol{P} \boldsymbol{\chi}, \tag{A.1}$$

where $\boldsymbol{\chi} \triangleq [e, \tilde{\psi}, \tilde{r}]^T$. The matrix $\boldsymbol{P}$ is defined as:

$$\boldsymbol{P} \triangleq \begin{bmatrix} \frac{1}{2} & 0 & 0 \\ 0 & \frac{\rho}{2}\left[\frac{k_\psi}{k_r}\left(1+\frac{1}{k_\psi}\right)+\frac{k_r}{k_\psi}\right] & \frac{\rho}{2k_\psi} \\ 0 & \frac{\rho}{2k_\psi} & \frac{\rho}{2k_r}\left(1+\frac{1}{k_\psi}\right) \end{bmatrix}, \tag{A.2}$$

where $\rho > 0$ is a constant parameter. The matrix $\boldsymbol{P}$ is symmetric and positive definite. Hence, its eigenvalues $\lambda_1, \lambda_2, \lambda_3$ are real and positive. In particular $\lambda_1 = 1/2$ and the other two are linearly dependent on ρ: $\lambda_2 = c_2(k_\psi, k_r)\rho$ and $\lambda_3 = c_3(k_\psi, k_r)\rho$, where $c_2(k_\psi, k_r) > 0$ and $c_3(k_\psi, k_r) > 0$. Therefore, by choosing $\rho > 0$ large enough, it is always possible to have $\lambda_m(\boldsymbol{P}) = 1/2$ and $\lambda_M(\boldsymbol{P}) = \rho \max(c_2, c_3)$ independently of the constants $k_\psi > 0$ and $k_r > 0$. In particular, with a big enough ρ, the following bound holds globally:

$$\frac{1}{2}||\boldsymbol{\chi}||^2 \leq V_3(\boldsymbol{\chi}) \leq \rho \max(c_2, c_3)||\boldsymbol{\chi}||^2. \tag{A.3}$$

On the domain $D \triangleq \{|e| \leq 1/\sigma\}$ the following bound holds for the time derivative $\dot{V}_3$:

$$\begin{aligned} \dot{V}_3 = -\rho\tilde{\psi}^2 - \rho\tilde{r}^2 - V_c e \sin(\sigma e) + \tilde{\psi}\ e\ h_e(e, \tilde{\psi}) \leq \\ \leq -\rho\tilde{\psi}^2 - \rho\tilde{r}^2 - V_c \sigma \frac{e^2}{2} + \tilde{\psi}\ e\ h_e(e, \tilde{\psi}). \end{aligned} \tag{A.4}$$

Without any loss of generality, ρ is chosen to satisfy $\rho > \max(2V_{\max},\ 2V_{\max}/\sigma)$. Therefore, since $|h_e(e, \tilde{\psi})| \leq 2V_{\max}$, as long as $\boldsymbol{\chi} \in D$ and $||\boldsymbol{\chi}|| \geq \mu \triangleq \frac{2V_{\max}}{\rho\sigma} > 0$ the bound (A.4) becomes:

$$\dot{V}_3 \leq -|\tilde{\psi}|\left(\rho|\tilde{\psi}| - 2V_{\max}|e|\right) - \rho\tilde{r}^2 - \frac{\sigma V_c}{2}e^2 < 0. \tag{A.5}$$

Notice that $\rho > \max(2V_{\max}, 2V_{\max}/\sigma)$ makes also sure that the ball $\mathcal{B}_\mu \triangleq \{||\boldsymbol{\chi}|| \leq \mu\} \subset D$. Finally, given the ball $\mathcal{B}_{1/\sigma} \triangleq \{||\boldsymbol{\chi}|| \leq 1/\sigma\} \subset D$, where $\mathcal{B}_\mu \subset \mathcal{B}_{1/\sigma}$ and $\mathcal{B}_{1/\sigma} \setminus \mathcal{B}_\mu \neq \emptyset$, the following inequality holds:

$$\mu < \frac{1}{\sigma}\sqrt{\frac{1}{2\rho \max(c_2, c_3)}}, \tag{A.6}$$

as long as the parameter $\rho > 0$ is chosen large enough to have $\lambda_m(\boldsymbol{P}) = 1/2$, $\lambda_M(\boldsymbol{P}) = \rho \max(c_2, c_3)$, and $\rho > \max(2V_{\max},\ 2V_{\max}/\sigma,\ 8V_{\max}^2 \max(c_2, c_3))$.

Therefore, according to Theorem 4.18 in Khalil (2000) or alternatively to Proposition 23 in Chaillet and Loría (2008), the solution $\boldsymbol{\chi}(t)$ of cascaded system (22) is uniformly ultimately bounded, with the following ultimate bound:

$$||\boldsymbol{\chi}(t)|| \leq \frac{2V_{\max}}{\sigma}\sqrt{\frac{2\max(c_2, c_3)}{\rho}}, \tag{A.7}$$

as long as the initial state $\boldsymbol{\chi}_o$ satisfies:

$$||\boldsymbol{\chi}_o|| \leq \frac{1}{\sigma}\sqrt{\frac{1}{2\rho \max(c_2, c_3)}}. \tag{A.8}$$

Notice that the ultimate bound (A.7) approaches zero as ρ becomes infinitely large and that (A.7) as well as (A.8) are linearly dependent on the parameter $1/\sigma$.

Appendix B

$$F_{u_r}(v_r, r) \triangleq \frac{1}{m_{11}}(m_{22}v_r + m_{23}r)r, \tag{B.1}$$

$$X(u_r) \triangleq \frac{m_{23}^2 - m_{11}m_{33}}{m_{22}m_{33} - m_{23}^2}u_r + \frac{d_{33}m_{23} - d_{23}m_{33}}{m_{22}m_{33} - m_{23}^2}, \tag{B.2}$$

$$Y(u_r) \triangleq \frac{(m_{22} - m_{11})m_{23}}{m_{22}m_{33} - m_{23}^2}u_r - \frac{d_{22}m_{33} - d_{32}m_{23}}{m_{22}m_{33} - m_{23}^2}, \tag{B.3}$$

$$\begin{aligned} F_r(u_r, v_r, r) \triangleq \frac{m_{23}d_{22} - m_{22}(d_{32} + (m_{22} - m_{11})u_r)}{m_{22}m_{33} - m_{23}^2}v_r \\ + \frac{m_{23}(d_{23} + m_{11}u_r) - m_{22}(d_{33} + m_{23}u_r)}{m_{22}m_{33} - m_{23}^2}r. \end{aligned} \tag{B.4}$$

The functions $h_{v_{\text{int}}}(v_{\text{int}}, \tilde{\psi})$ and $h_e(e, \tilde{\psi})$ are:

$$\begin{aligned} h_{v_{\text{int}}}(v_{\text{int}}, \tilde{\psi}) \triangleq -\frac{1 - \cos(\tilde{\psi})}{\tilde{\psi}}\left(V_x \sin(\sigma v_{\text{int}}) + V_y \cos(\sigma v_{\text{int}})\right) \\ - \frac{\sin(\tilde{\psi})}{\tilde{\psi}}\left(V_x \cos(\sigma v_{\text{int}}) - V_y \sin(\sigma v_{\text{int}})\right), \end{aligned} \tag{B.5}$$

$$h_e(e, \tilde{\psi}) \triangleq V_c\frac{1 - \cos(\tilde{\psi})}{\tilde{\psi}}\sin(\sigma e) + V_c\frac{\sin(\tilde{\psi})}{\tilde{\psi}}\cos(\sigma e), \tag{B.6}$$

where the limits of $h_{v_{\text{int}}}$ and h_e for $\tilde{\psi} \to 0$ exist and are finite. The constant $V_c > 0$ is the magnitude of the current: $V_c \triangleq \sqrt{V_x^2 + V_y^2}$. Notice that the following identities are used when moving the equilibrium point $v_{\text{int},1}^{\text{eq}}$ to the origin in Section 6 (recall that $e = v_{\text{int}} - v_{\text{int},1}^{\text{eq}}$):

$$V_x \sin(\sigma v_{\text{int}}) + V_y \cos(\sigma v_{\text{int}}) = -V_c \sin(\sigma e), \tag{B.7}$$

$$V_x \cos(\sigma v_{\text{int}}) - V_y \sin(\sigma v_{\text{int}}) = -V_c \cos(\sigma e), \tag{B.8}$$

$$\sin(\text{atan2}(V_y, V_x)) = V_y/V_c, \tag{B.9}$$

$$\cos(\text{atan2}(V_y, V_x)) = V_x/V_c. \tag{B.10}$$